PERGAMON

International Journal of Solids and Structures 36 (1999) 1985–2014

INTERNATIONAL JOURNAL OF SOLIDS and STRUCTURES

A crack bridging model for bonded plates subjected to tension and bending

C. H. Wang*, L. R. F. Rose

Aeronautical and Maritime Research Laboratory, Defence Science and Technology Organisation, Melbourne, Australia

Received 6 November 1997; in revised form 2 February 1998

Abstract

A crack bridging model is presented for analysing the tensile stretching and bending of a cracked plate with a patch bonded on one side, accounting for the effect of out-of-plane bending induced by load-path eccentricity inherent to one-sided repairs. The model is formulated using both Kirchhoff–Poisson plate bending theory and Reissner's shear deformation theory, within the frameworks of geometrically linear and nonlinear elasticity. The bonded patch is represented as distributed springs bridging the crack faces. The springs have both tension and bending resistances; their stiffness constants are determined from a one-dimensional analysis for a single strap joint, representative of the load transfer from the cracked plate to the bonded patch. The resulting coupled integral equations are solved using a Galerkin method, and the results are compared with three-dimensional finite element solutions. It is found that the formulation based on Reissner's plate theory provides better agreement with finite element results than the classical plate theory.

Nomenclature

a	half crack length
c_{ij}	elements of spring compliance matrix ($i = 1, 2$)
E	Young's modulus
G	strain energy release rate
h_1	normalised crack opening displacement (u/a)
h_2	normalised generalised crack face rotation displacement ($\frac{1}{6}\theta t_P/\alpha$)
I	moment of inertia
k_α	spring stiffness matrix ($\alpha = t, b$ where t denotes tension and b denotes bending)
K	stress intensity factor
$K_b^{(K)}$	bending stress intensity based on Kirchhoff–Poisson plate theory

* Corresponding author. Fax: 00 613 9626 7089; e-mail: chun.hui.wang@dsto.defence.gov.au

0020–7683/99/$ - see front matter
PII: S0020–7683(98)00070–5

$K_b^{(R)}$ bending stress intensity based on Reissner's plate bending theory
M bending moment
N membrane force
S stiffness ration ($E'_R t_R / E'_P t_P$)
t thickness
u crack face displacement (mid-plane)
$\bar{z}$ position of the neutral plane of a plate.

Greek symbols
θ crack face rotation
μ shear modulus
ν Poisson's ratio
σ_0 prospective stress at the crack location
σ_m membrane stress
σ_b maximum bending stress.

Subscripts
P, R, A denoting parameters pertaining to the plate, the reinforcement, and the adhesive layer.

Superscripts
∞ parameters pertaining to the remote loading.

1. Introduction

With the increasing use of bonded repair techniques for repairing cracks and other damages in primary airframe structures, the design and evaluation of bonded repairs is becoming a major concern to meet certification requirements of damage tolerant repairs to critical structures (Baker, 1997). A critical repair is defined as one in which the residual strength of the unrepaired component would be lower than the design ultimate or, even worse, the design limit load. To certify critical repairs to primary structures we need to be able to demonstrate by analysis and/or test that the repair can meet the residual strength and damage tolerance requirements. To ensure adequate damage tolerance of the repaired structure, it is essential to determine the reduction in the stress intensity factor after repair so as to ensure that (i) the residual strength has been restored to an acceptable level, and (ii) the growth rate of the crack under fatigue condition is sufficiently slow to ensure an acceptable residual life, or inspection interval.

A bonded repair, which involves adhesively bonding a composite patch to a cracked or damaged structure, may fail in a number of modes, such as patch failure, failure of the adhesive layer, failure of the plate outside the repair region due to stress elevation near the termination of the patches, or insufficient reduction in the stress intensity factor of the crack thus leading to continuous crack growth. Over the past two decades analytical procedures (Erdogan and Arin, 1972; Keer et al., 1976; Rose, 1981, 1982, 1988) have been developed to address these issues, assuming that the bonded structure is under tension only and there is no secondary bending. In particular, the simple, closed form solution derived by Rose (1981, 1982, 1988) for the limiting value of the stress intensity factor has played a key role in the development of bonded repair methodology, which has been

supported by extensive laboratory testing and validation (Baker and Jones, 1988; Baker 1993; Rose et al., 1995). More recently it has been noted that the original expressions derived by Rose for two-sided repairs need to be modified to account for the plane strain state along the crack length direction (Wang and Rose, 1998).

Since most often only one face of a structure to be repaired is accessible and sometimes only one side of a structure is allowed to be patched for other reasons, one-sided repairs are often adopted in practical applications. In this case if the structure is well supported against out-of-plane deflection, for example, by stiffeners attached to one side of the structure, only the tensile stretching of the crack needs to considered, allowing the problem to be solved using relatively simple methods (Erdogan and Arin, 1972; Keer et al., 1976; Rose, 1981, 1982; 1987). However, there are many cases where the structures to be repaired are not restrained from out-of-plane deflection, and the bonding of a single patch on one surface will cause the load-path to become eccentric, resulting in secondary bending near the crack region (Ratwani, 1979; Jones, 1983; Rose, 1988; Arendt and Sun, 1994; Wang et al., 1998). Nevertheless, it has been shown that the total strain energy release rate and the (root-mean-square) stress intensity factor of a one-sided repaired crack will asymptote to, but never exceeds, a limiting value as the crack length increases (Callinan et al., 1997; Wang et al., 1998). Based on a geometrically linear analysis, Wang et al. (1998) have derived an upper bound solution of the strain energy release rate, which has been shown to compare well with three-dimensional finite element results (Callinan et al., 1997).

Previous work has also highlighted two major difficulties in predicting theoretically the efficiencies of unsupported one-sided repairs. First, although the total strain energy release rate for a semi-infinite crack can be determined by an energy method, this method alone is insufficient to partition the total strain energy release rate into a tension and bending component (Wang and Rose, 1997). Consequently the exact values of the membrane and bending stress intensity factors are unknown, nor is the maximum stress intensity factor, which is probably the most important parameter dictating the residual strength and potential fatigue crack growth rate. Secondly, to quantify the effect of crack length on the repair efficiency, a more detailed stress analysis is called for to determine the stress intensity factors for varying crack lengths, which is of great importance when either debonding or crack growth is the rate-determining process.

The main purpose of this article is to present an analytical method for the combined tensile stretching and bending of one-sided repairs. The patch is replaced by distributed springs bridging the crack faces. The springs have tension and bending resistances. Both Kirchhoff–Poisson plate bending theory and Reissner's shear deformation theory will be employed, in conjunction with the generalised plane stress theory for tensile stretching, to formulate the governing equations. To account for the geometrically non-linear deformation of a one-sided repair subjected to tensile loads, a hybrid method is proposed in which the prospective stresses along the crack path are analysed using geometrically non-linear plate theories, whereas the perturbation problem is solved within the framework of geometrically linear elasticity. The resulting solutions are shown to provide upper bounds to all the fracture parameters.

2. Basic formulation

Referring to Fig. 1, the problem to be considered is a cracked plate repaired by a patch adhesively bonded on one side. The plate, which has a thickness of t_P, contains a through crack of length $2a$.

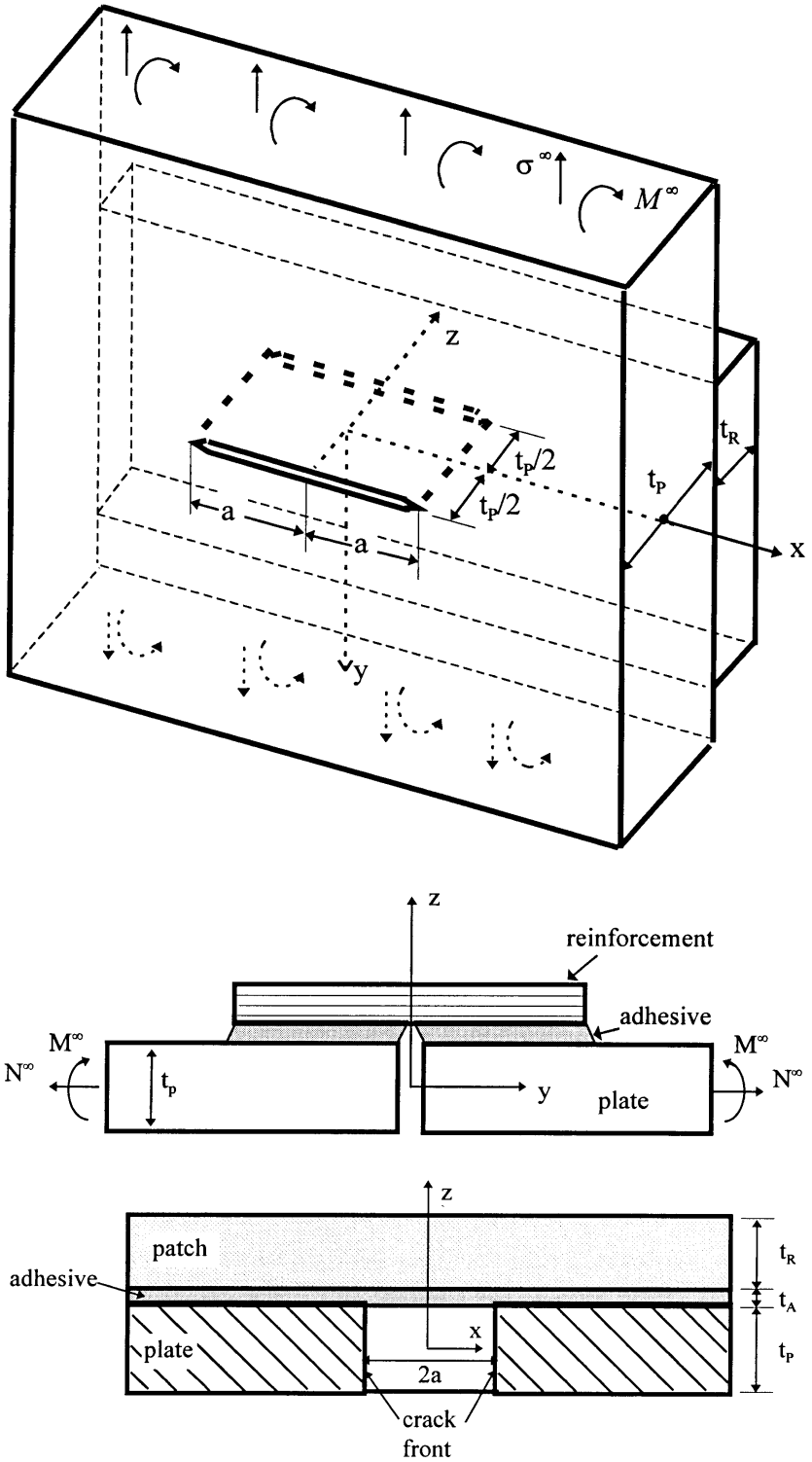

Fig. 1. (a) A cracked plate reinforced by a patch attached to one surface. (b) Cross-section in the y–z plane ($-a < x < a$). (c) Cross section in the x–z plane ($y = 0$).

The thickness of the patch and the adhesive layer are respectively t_R and t_A. The cross-sections in the y–z and x–z planes are depicted in Fig 1(b) and (c). The Young's modulus and the Poisson's ratio of each individual layer are denoted as E and v; here and in the following subscripts P, R, and A will be used to distinguish properties pertaining, respectively, to the plate, the reinforcement and the adhesive layer.

At remote distance from the repaired region, the plate is subjected to a combined tension in the y-direction and a pure bending about the x-axis. The boundary conditions for the problem are that the crack surfaces are stress free and there is a prescribed stress system at the infinity so that

$$\sigma_{yy} \to \sigma^{\infty}, \quad M_{xx} \to M^{\infty} \quad \text{as} \sqrt{x^2+y^2} \to \infty \quad (-t_P/2 < z < t_P/2) \tag{1a}$$

and

$$\sigma_{yy} = \tau_{xy} = 0 \quad (|x| < a, \quad y = 0, \quad -t_P/2 < z < t_P/2) \tag{1b}$$

By using the superposition principle it is easy to demonstrate that the problem depicted in Fig. 1(a) is equivalent to solving the following perturbation problem as depicted in Fig. 2,

$$\text{plate}: \begin{cases} \sigma_{yy} = -\sigma_0(z) & (|x| < a, y = 0, -t_P/2 \leqslant z < t_P/2) \\ u_y = \dfrac{\mathrm{d}u_y}{\mathrm{d}z} = 0 & (|x| \geqslant a, y = 0, -t_P/2 \leqslant z < t_P/2) \\ \sigma_{xx} \to 0, \quad \sigma_{yy} \to 0, \quad \tau_{xy} \to 0 & (\sqrt{x^2+y^2} \to \infty, -t_P/2 \leqslant z < t_P/2) \end{cases} \tag{2a}$$

$$\text{patch}\, u_y = \frac{\mathrm{d}u_y}{\mathrm{d}z} = 0 \quad (|x| < \infty, \quad y = 0, t_P/2 + t_A \leqslant z < t_P/2 + t_A + t_R) \tag{2b}$$

where $\sigma_0(z)$ is the stress distribution along the prospective crack path in the uncracked structure (with reinforcement), which will be determined in Section 3.

By treating the cracked plate and the patch as thin plates, the stress distribution on the crack faces can be considered as the superposition of a membrane force N_0 and a bending moment M_0, with the stress distribution being given by $\sigma_0(z) = -(N_0/t_P - 12M_0 z/t_{Pq}^3)$. Without the bonded patch, it is obvious that $N = N^{\infty}$ and $M_0 = M^{\infty}$. After patching, however, the stresses along the prospective crack path are no longer equal to those prior to the application of reinforcement.

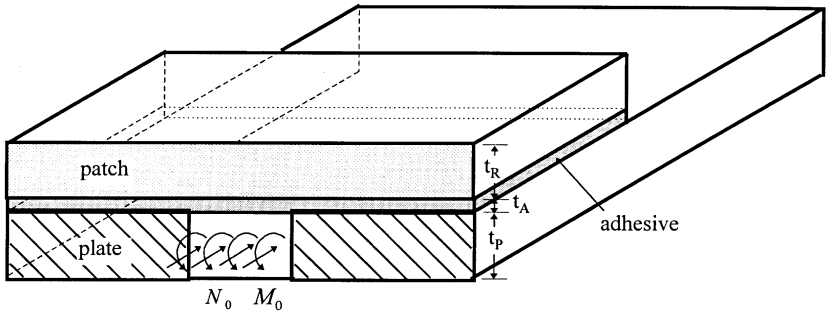

Fig. 2. Perturbation problem of repaired cracked plate subjected to tension and bending.

Furthermore, as a result of bonding a patch on one side only, the repaired structure now experiences a load-path eccentricity, leading to geometrically non-linear deformation. Consequently, the stress $\sigma_0(z)/\sigma^\infty$ would depend on the applied load levels. In the present work, the stress distribution $\sigma_0(z)$ in the plate along the prospective crack path will be first determined in Section 3, within the geometrically linear and geometrically non-linear elasticity frameworks. Then the perturbation problem of a crack pressurised by a combination of membrane force and bending moment is solved using a crack bridging model as detailed in Section 5, within the framework of geometrically linear elasticity. Then a hybrid method is proposed in Section 7 to obtain an upper-bound solution to the tension and bending stress intensity factors.

If we denote the membrane force and the bending moment acting on the prospective crack path as N_0 and M_0, and denote the crack surface displacement and rotation as u and θ (all referred to the mid-plane of the cracked plate). The basic idea underlying the crack bridging model to be described below is that (i) by representing the effect of the reinforcement by an infinite number of tension and bending springs bridging the crack faces, and (ii) by deriving the relationship between (N_0, M_0) and (u, θ) from an analysis of a single strap joint in plane strain (Fig. 1(b)), one can model the problem depicted in Fig. 2 as a plate containing a through crack reinforced by distributed tension and bending springs; see Fig. 3. Thus, a complicated three-dimensional problem is reduced to a two-dimensional problem of a bridged crack, and a one-dimensional problem to determine the crack bridging traction law, which will be presented in Section 4. The resulting hyper-singular integral equations are then solved using a Galerkin method, which is detailed in Section 6.

To a certain degree the proposed crack bridging model is similar in spirit to the line spring model developed by Rice and Levy (1972) for plates with part-through cracks, where the net ligament was modelled as tension and bending springs, and the spring compliance matrix was

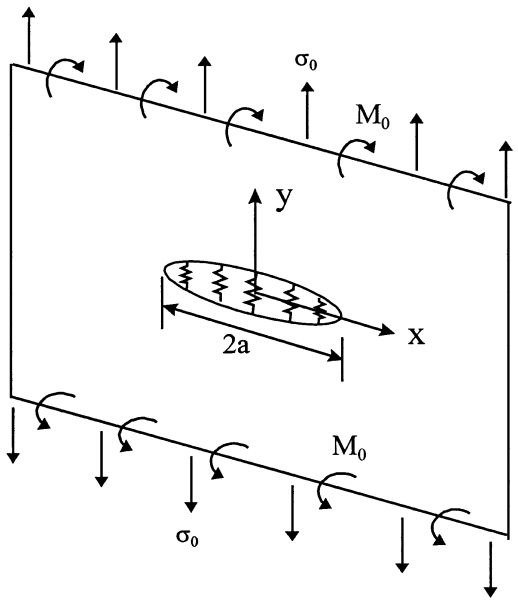

Fig. 3. A plate with a through crack reinforced with tension and bending springs.

determined by making use of the known solution of a strip with an edge crack subjected to remote tension and bending. However, one distinct difference between the present crack bridging method and the line spring model is that in the line spring model a plate with part-through crack is modelled as a plate containing a through crack, with the crack being reinforced with tension and bending springs. In the present case, however, the reinforcement is removed and replaced by tension and bending springs bridging the crack faces, assuming that the stress diffusion between the cracked plate and the reinforcement occurs over a negligible distance hence the patch can be removed and replaced by distributed springs having tension and bending resistance. Such an approach has been (Wang and Rose, 1998) shown to reproduce the solution of an exact formulation based on elasticity theory by Keer et al. (1976), for symmetric repairs, when the characteristic distance over which the load transfer occurs is far smaller than the characteristic crack length.

Another major difference between the present crack bridging model and the line spring method for part-through crack problem is that the crack front in the present case is perpendicular to the plate surface, and hence the 'ligament' ahead the crack front would be infinite rather than finite as in the part-through crack case. Therefore the method of determining the compliance matrix used in the line spring model is not applicable to bonded repairs.

3. Prospective stress distribution

Let us assume that the reinforcement spans across the entire width of the plate, so that the stresses in the reinforcement and the plate are uniform in the x-direction everywhere within the reinforced portion, and there is no debonding between the plate and the reinforcement. The offset in the load-path of the membrane force as indicated in Fig. 4(a) will induce a bending moment, which will cause the neutral plane of the reinforced portion to move towards the load-path (see Fig. 4(b)), and this will in turn relieve the bending moment. Therefore strictly speaking the geometrically nonlinear deformation behaviour must be taken into account. Nevertheless, a geometrically linear solution will provide a conservative estimate of the stresses in the plate and the reinforcement. In the present study, both geometrically linear and nonlinear solutions will be derived which would provide an upper and lower bound to the actual stress distribution.

3.1. Geometrically linear solution

Assuming that the reinforcement is far greater than the shear stress transfer length, we can neglect the influence of the outer edge of the reinforcement and treat the reinforced region as a composite plate with a rigid bondline. The stress distribution in the plate and the reinforcement can be determined using the well-known composite plate theory (Gere and Timoshenko, 1987). The position of the neutral plane of the composite plate consisting of the base plate and the rigidly-bonded reinforcement is denoted by $\bar{z}$, referring to Fig. 4,

$$\bar{z} = \frac{S(t_P + t_R)}{2(1+S)} \tag{3}$$

where S denotes the stiffness ratio, $S = E'_R t_R / E'_P t_P$, and E' refers to the plane-strain Young's modulus ($E' = E/(1-\nu^2)$). The moment of inertial of the reinforced region I_t, is

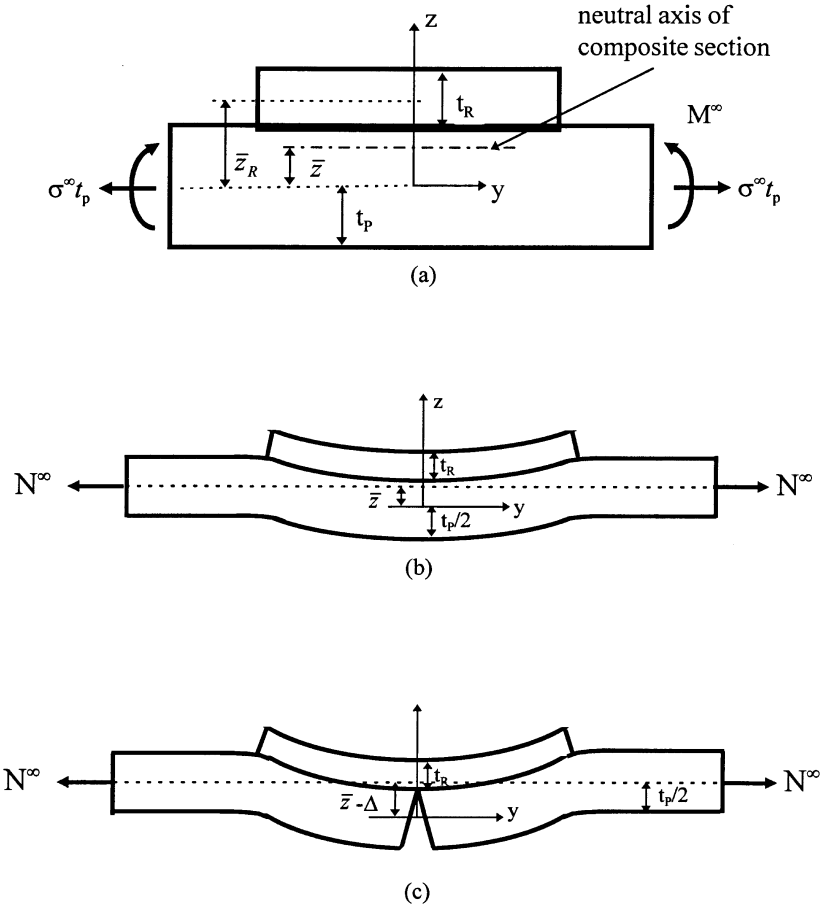

Fig. 4. Prospective stress distribution in the plate : (a) geometrically linear analysis ; (b) geometrically non-linear analysis ; and (c) deformed shape of a single strap joint.

$$I_t = I_P + nI_R \tag{4}$$

where

$$I_P = t_P^3/12 + t_P\bar{z}^2, \quad I_R = t_R^3/12 + (t_P + t_R - 2\bar{z})^2/4 \quad \text{and} \quad n = E'_R/E'_P$$

The stress distribution in the patched plate is assumed to be linear in the thickness direction, so that it can be specified in terms of a membrane force N_0 and a bending moment M_0 per unit length in the x-direction, which act on the plane $y = 0$ containing the crack (see Wang et al., 1998, noting the use of different coordinate system). This implies that the prospective stress is given by

$$\sigma_0(z) = \frac{\sigma^\infty}{1+S} + \frac{[\sigma^\infty t_P\bar{z} + M^\infty](\bar{z} - z)}{I_t} = \sigma_m - \sigma_b\frac{2z}{t_P} \quad (-t_P/2 < z < t_P/2) \tag{5}$$

where σ_m denotes the membrane stress and σ_b the maximum bending stress (negative on the inner

surface close to the bondline). Consequently the membrane force and bending moment can be expressed as

$$N_0 = \int_{-t_P/2}^{t_P/2} \sigma_{yy}(y=0,z)\,\mathrm{d}z \equiv \frac{\sigma^\infty t_P}{1+S} + \frac{\sigma^\infty t_P^2 \bar{z}^2 + M^\infty t_P \bar{z}}{I_t} \tag{6}$$

$$M_0 = -\int_{-t_P/2}^{t_P/2} \sigma_{yy}(y=0,z) z\,\mathrm{d}z \equiv [\sigma^\infty t_P \bar{z} + M^\infty] \frac{t_P^3}{12 I_t} \tag{7}$$

It is thus clear due to the load-path offset, there exists a non-zero prospective bending moment even when the plate is subjected to only a remote tension.

3.2. Geometrically non-linear solution

Since the membrane force exerts a restoring force to move the neutral plane of the reinforced region towards the load line, as illustrated in Fig. 4(b), the actual bending moment will be less than determined on the basis of geometrically linear analysis. This problem has been treated by Rose (1988) for the case of finite reinforcement, and his results suggested that for infinite overlap, the neutral plane of the reinforced region will align exactly with the load line for non-vanishing remote tensile load. This means that if the structure is subjected to a remote tension only, the stresses in the plate and the reinforcement will be uniform in the z-direction, at $y = 0$. Thus, for this limiting case of an infinite overlap, the prospective membrane force N_0 and the bending moment M_0 can be determined from eqns (6) and (7) by equating the neutral plane offset $\bar{z}$ to zero, i.e.,

$$N_0 = \frac{\sigma^\infty t_P}{1+S} + \frac{M^\infty t_P \bar{z}}{I_t} \tag{8}$$

$$M_0 = M^\infty \frac{t_P^3}{12 I_t} \tag{9}$$

As discussed earlier, the problem to be solved can be reduced to a perturbation problem where the above determined membrane force and bending moment are applied to the crack faces. It should be pointed out that in the case when the plate is subjected to remote tension only, although the prospective stress distribution through the plate thickness is uniform, the unrestricted out-of-plane deflection near the crack region will result in a bending stress intensity factor along the crack front as well as a membrane stress intensity factor; further discussion will be presented later.

4. Determination of spring constants

In order to formulate a crack bridging model, it is essential to determine first the spring constants. As depicted in Fig. 5(a), let us denote the crack face displacement and rotation as u and θ, in relation to the mid-plane of the plate, caused by the application of a membrane force N_0 and bending moment M_0. The relationship between (N_0, M_0) and (u, θ) can be determined by analysing

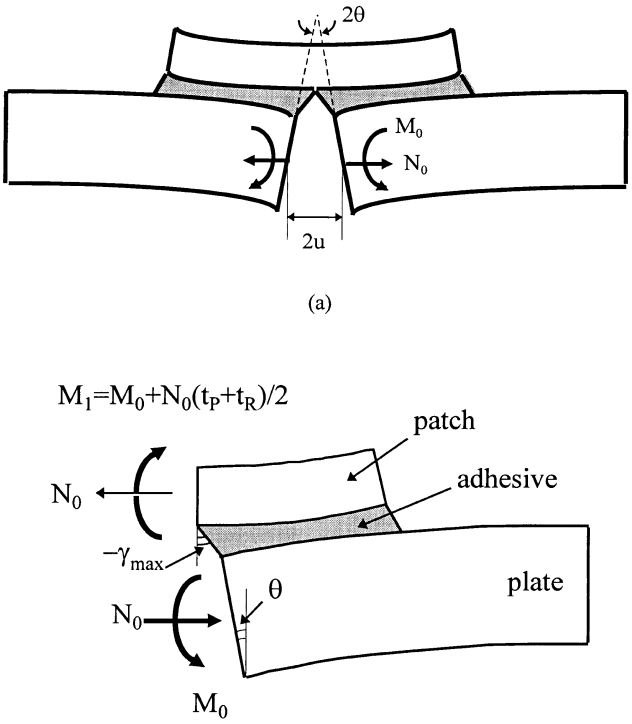

Fig. 5. (a) Single strap joint representing one-sided repairs subjected to membrane tension and bending moment, and (b) notations and boundary conditions.

the single strap joint under plane strain conditions; details are presented in Appendix A. When expressed in a matrix form, we have

$$\begin{Bmatrix} u \\ \theta \end{Bmatrix} = \begin{bmatrix} c_{11} & c_{12} \\ c_{21} & c_{22} \end{bmatrix} \begin{Bmatrix} N_0 \\ M_0 \end{Bmatrix} \tag{10}$$

where c_{ij} are given in Appendix A. From equation (10) on can obtain the stiffness matrix,

$$\begin{Bmatrix} N_0 \\ M_0 \end{Bmatrix} = \begin{bmatrix} d_{tt} & d_{tb} \\ d_{bt} & d_{bb} \end{bmatrix} \begin{Bmatrix} u \\ \theta \end{Bmatrix} \tag{11}$$

where

$$\begin{aligned} d_{tt} &= c_{22}/\Delta, \quad d_{tb} = -c_{21}/\Delta \\ d_{bt} &= -c_{12}/\Delta, \quad d_{bb} = c_{11}/\Delta \\ \Delta &= c_{11}c_{22} - c_{12}c_{21} \end{aligned} \tag{12}$$

To facilitate the following analysis it is advantageous to express the spring traction law in terms of the generalized displacements corresponding to the membrane stress σ_m $(=N_0/t_P)$ and the

maximum bending stress σ_b ($=6M_0/t_P^2$). Since the total strain energy release rate per unit thickness is given by

$$G = \sigma_m u + \tfrac{1}{6}\sigma_b \theta t_P \tag{13}$$

it is clear that the associated generalised placements are, respectively, u and $\theta t_P/6$. From eqn (11) we can express the relationship between (σ_m, σ_b) and $(u, \theta t_P/6)$ as

$$\begin{Bmatrix} \sigma_m \\ \sigma_b \end{Bmatrix} = E_P \begin{bmatrix} k_{tt} & k_{tb} \\ k_{bt} & k_{bb} \end{bmatrix} \begin{Bmatrix} u \\ \frac{1}{6}\theta t_P \end{Bmatrix} \tag{14}$$

where k_{ij} represent spring constants which have a unit of length^{-1},

$$k_{tt} = \frac{1}{E_P t_P} \mathrm{d}_{tt} \equiv \frac{c_{22}}{E_P t_P \Delta} \quad k_{tb} = \frac{6}{E_P t_P^2} d_{tb} \equiv -\frac{6c_{21}}{E_P t_P^2 \Delta} \tag{15a}$$

$$k_{bt} = \frac{6}{E_P t_P^2} d_{bt} \equiv -\frac{6c_{12}}{E_P t_P^2 \Delta} \quad k_{bb} = \frac{36}{E_P t_P^3} d_{bb} \equiv \frac{36c_{11}}{E_P t_P^3 \Delta} \tag{15b}$$

According to elastic reciprocity we should have $k_{tb} = k_{bt}$. However, due to the approximate nature of the plate theory employed in the present work the cross terms c_{12} and c_{21} as given in Appendix A are not exactly identical but the numerical difference is relatively small. It is also possible to symmetrise the spring stiffness matrix is required,

$$k_{tb}^* = k_{bt}^* = \frac{k_{tb} + k_{bt}}{2} \tag{16}$$

which is the only permissible symmetrisation to ensure the equivalence in the total energy release rate.

5. Crack bridging model

The basic idea of a crack bridging model is to model the patching problem as a single plate with a through crack reinforced by distributed tension and bending springs sprung over the crack faces, where the spring constant matrix has already been obtained in Section 4. The crack bridging problem depicted in Fig. 3 is similar to the 'line spring' model introduced by Rice and Levy (1972) to deal with part-through surface cracks in homogeneous plates. Here the tension and bending fields are coupled by the boundary condition along the line of discontinuity, which relate the crack face displacement u and rotation θ to the membrane force N_0 and the bending moment M_0. Noting eqn (11), the boundary conditions along $y = 0$ can be expressed in terms of the yet unknown displacement and rotation,

$$N_{yy}(x, 0^+) = -N_0 + d_{tt} u(x) + d_{tb} \theta(x) \quad (-a < x < a) \tag{17a}$$

$$M_{xx}(x, 0^+) = -M_0 + d_{bt} u(x) + d_{bb} \theta(x) \quad (-a < x < a) \tag{17b}$$

Making use of the solution of the in-plane displacement of a bridged crack under tension (see

Joseph and Erdogan, 1987, 1989; Nemat-Nasser and Hori, 1987), the unknown crack face displacement (one half of the total crack opening displacement) can be expressed as,

$$\frac{E_P t_P}{2\pi}\int_{-a}^{a}\frac{u(\xi)}{(x-\xi)^2}\,d\xi = N_{yy}(x_1,0^+) \equiv -N_0 + d_{tt}u(x) + d_{tb}\theta(x) \tag{18}$$

The integral in the above equation is interpreted as a Hadamard finite part (Hadamard, 1952), which can be viewed as the derivative of a Cauchy principal value integral. Despite the higher order of singularity in the integrand, the present formulation has many advantages over that based on the derivative of the displacement, or dislocation density, mainly because the unknown displacement function is bounded unlike the density function which is singular near the crack tip. Numerical methods and convergence for this class of strongly singular integral equations have been investigated by a number of authors (Frenkel, 1983; Golberg, 1983, 1985; Kaya and Erdogan, 1987; Joseph and Erdogan, 1987; Ervin and Stephan, 1992) and it has been found that the hypersingular integral equations can be efficiently solved by using either Galerkin's method or collocation methods.

Since the cross terms d_{tb} and d_{bt} are non-zero, the membrane resistance of the distributed springs is dependent on not only the crack face displacement but also the crack face rotation. Therefore the tensile stretching of the crack is coupled with the bending, and vice versa. To quantify the bending deformation of a plate, we need to adopt a plate theory. In this regard, Kirchhoff–Poisson plate bending theory (Timoshenko and Woinowsky-Krieger, 1958) and Reissner's shear deformation theory (Reissner, 1947) are probably the most widely used plate theories. Due to the inability of Kirchhoff–Poisson plate theory to completely satisfy stress free boundary conditions along the crack face, it leads to not only misleading stress intensity factor but also incorrect angular distribution of the asymptotic stress state near the crack tip (Williams, 1961). This problem has led to the use of Reissner's plate theory (Knowles and Wang, 1960; Hartranft and Sih, 1968; Wang, 1968) for describing the crack tip fields, leaving aside the uncertainty of the perturbed stress state on the plate surface (Sih, 1971).

Due to the use of higher order differential equations, the analysis based on Reissner's plate theory is considerably more complicated than that based on the classical plate theory. For a single plate containing a long through crack ($a/t_P \to \infty$), the expenses of using a much more complicated Reissner's plate theory may overweigh the gain of improved accuracy. This is because the classical plate theory would correctly predict the strain energy release rate in the long crack limit, identical to that obtained from Reissner's plate theory (Hui and Zehnder, 1993). Hence there exists a universal relationship between the stress intensity factor from Reissner's plate theory and that from the classical plate theory,

$$K_b^{(R)} = \sqrt{\frac{1+\nu_P}{3+\nu_P}}\,K_b^{(K)} \tag{19}$$

where $K_b^{(R)}$ and $K_b^{(K)}$ denote, respectively, the bending stress intensity factors determined from Reissner's plate theory and Kirchhoff–Poisson plate theory (no crack closure in the compression side is assumed; this issue will be dealt with separately in another article). It is, however, not clear whether the same relationship still holds for a cracked plate repaired on one side. To clarify this point, both plate theories will be employed in the following analyses.

5.1. Kirchhoff–Poisson plate bending theory

Referring to equations (17) and making use of the solutions for a single plate with a through crack based on Kirchhoff–Poisson plate theory (Joseph and Erdogan, 1987), the following hyper-singular integral equation can be obtained,

$$\frac{3+\nu_P}{1+\nu_P}\frac{E_P t_P^3}{24\pi}\int_{-a}^{a}\frac{\theta(t)}{(x-\xi)^2}\,d\xi = M_{xx}(x,0^+) \equiv -M_0 + d_{bt}u(x) + d_{bb}\theta(x) \tag{20}$$

which, together with eqn (18), furnishes a set of coupled integral equations.

For the purpose of parametric investigation, we introduce the following non-dimensional variables,

$$h_1(x) = u(x)/a \tag{21}$$

$$h_2(x) = \tfrac{1}{6}\theta t_P/a. \tag{22}$$

The integral eqns (18), (20) can thus be normalised to become

$$-\frac{1}{2\pi}\int_{-1}^{1}\frac{h_1(\eta)}{(r-\eta)^2}\,d\eta + (k_{tt}a)h_1(r) + (k_{tb}a)h_2(r) = \frac{\sigma_m}{E_P} \tag{23a}$$

$$-\frac{3+\nu_P}{1+\nu_P}\frac{3}{2\pi}\int_{-1}^{1}\frac{h_2(\eta)}{(r-\eta)^2}\,d\eta + (k_{bt}a)h_1(r) + (k_{bb}a)h_2(r) = \frac{\sigma_b}{E_P} \tag{23b}$$

where $r = x/a$, $\eta = \xi/a$.

The coupled integral equations (23) have no closed form solutions. However, their solutions can be readily obtained numerically using a Galerkin method: expand the unknown functions in terms of Chebyshev polynomials and then determine the coefficients numerically, similar to the approach used by Nemat-Nasser and Hori (1987) for the case of tension springs only. Details will be shown in the next section. It may be shown that the following functions are also bounded everywhere within $(-1, 1)$,

$$\bar{h}_{1,2}(r) = \frac{h_{1,2}(r)}{\sqrt{1-r^2}} \tag{24}$$

Furthermore, the left-hand sides in eqns (23) give the membrane and bending stresses outside the cut $(-1, 1)$, which are singular near $r \to 1^+$ or $r \to -1^-$. By using the following asymptotic behaviour for $r \to 1^+$,

$$\lim_{r\to 1^+}\frac{1}{2\pi}\int_{-1}^{1}\frac{f(\eta)\sqrt{1-\eta^2}}{(r-\eta)^2}\,d\eta = \lim_{r\to 1^+}\frac{f(1)}{2\sqrt{2(r-1)}} \tag{25}$$

where f denotes any bounded function within $(-1, 1)$. It is easily shown that the membrane stress intensity factor is given by

$$K_m = \lim_{r\to 1^+}\sqrt{2\pi a(r-1)}\,\sigma_{yy}(r,0) = \frac{E_P\sqrt{\pi a}}{2}\bar{h}_1(1) \tag{26}$$

Similarly the bending stress intensity factors based on Kirchhoff–Poisson plate theory (using stress definition) is,

$$K_b^{(K)} = \frac{3+\nu_P}{1+\nu_P}\frac{3E_P\sqrt{\pi a}}{2}\bar{h}_2(1). \tag{27}$$

It should be noted that when the Kirchhoff–Poisson plate theory is employed, the displacement based definition will lead to an answer different from eqn (27). However, since Kirchhoff–Poisson plate theory is a stress based formulation, the stress definition of the bending stress intensity factor (no crack closure is considered) is perhaps the only valid definition and displacement based definition will not be discussed further.

5.2. Reissner's plate theory

Similarly, the crack face rotation for a bridged crack subjected to bending is given by (Joseph and Erdogan, 1989),

$$\frac{E_P t_P^3}{24\pi}\int_{-a}^{a}\frac{\theta(\xi)}{(x-\xi)^2}\,d\xi + \frac{5}{1+\nu_P}\frac{E_P t_P}{24\pi}\int_{-a}^{a}L(s)\theta(\xi)\,d\xi = M_{xx}(x,0^+) \tag{28}$$

where

$$s = \sqrt{10}|x-\xi|/t_P \tag{29a}$$

$$L(s) = -\frac{48}{s^4}+\frac{4}{s^2}+4[K_2(s)-K_0(s)]+\frac{24}{s^2}K_2(s) \tag{29b}$$

and K_0 and K_2 are the modified Bessel functions of the second kind. It can be shown (Joseph and Erdogan, 1987) that $L(s)$ is a Fredholm kernel with only a logarithmic singularity near $s=0$ (proof is given in Appendix B, with corrections to reference Joseph and Erdogan (1987)).

By adopting the normalisation introduced earlier, the integral equations (18), (28) can be normalised to become,

$$-\frac{1}{2\pi}\int_{-1}^{1}\frac{h_1(\eta)}{(r-\eta)^2}\,d\eta + (k_{tt}a)h_1(r)+(k_{tb}a)h_2(r) = \frac{\sigma_m}{E_P} \tag{30a}$$

$$-\frac{3}{2\pi}\int_{-1}^{1}\frac{h_2(\eta)}{(r-\eta)^2}\,d\eta - \frac{15}{(1+\nu_P)2\pi}\left(\frac{a}{t_P}\right)^2\int_{-1}^{1}L\left(\sqrt{10}\frac{a}{t_P}|r-\eta|\right)h_2(\eta)\,d\eta + (k_{bt}a)h_1(r)+(k_{bb}a)h_2(r) = \frac{\sigma_b}{E_P} \tag{30b}$$

while the membrane stress intensity factor is still given by eqn (26), the bending stress intensity factor can be derived either using stress based definition or displacement based definition (which will yield identical answer),

$$K_b^{(R)} = \frac{3E_P\sqrt{\pi a}}{2}\bar{h}_2(1) \tag{31}$$

Since Reissner's plate theory yields the same angular distribution of the asymptotic stress state as given by elasticity theory, we can define a stress intensity factor at coordinate z through the plate thickness,

$$K(z) = K_m - \frac{2z}{t_P}K_b$$

whereas this is not the case for Kirchhoff–Poisson plate theory.

6. Numerical methods

An effective way of solving the hyper-singular equations, numerically, is provided by expanding the unknowns using Chebyshev polynomials of the second kind, U_i:

$$h_1(r) = W(r)\bar{h}_1(r) \cong W(r)\sum_{i=0}^{N} f_i U_i(r) \tag{32}$$

$$h_2(r) = W(r)\bar{h}_2(r) \cong W(r)\sum_{i=0}^{N} g_i U_i(r) \tag{33}$$

where $W(r) = \sqrt{1-r^2}$, f_i and g_i $(i = 0, 1, 2, \ldots, N)$ are coefficients yet to be determined. Here N is selected to be sufficiently large to ensure convergence within an acceptable accuracy. The method is effective because, with this expansion, the hyper-singular integral can be evaluated analytically, e.g.,

$$\int_{-1}^{1} \frac{W(r)U_i(r)\,\mathrm{d}r}{(x-r)^2} = -\pi(i+1)U_i(x) \quad (-1 < x < 1) \tag{34}$$

One can now develop a Galerkin-type method to determine the unknown coefficients (f_i and g_i).

6.1. Classical plate theory

Making use of eqn (34), eqns (23) can be written as

$$\sum_{i=0}^{N}\frac{(i+1)}{2}f_iU_i(r) + W(r)(k_{tt}a)\sum_{i=0}^{N}f_iU_i(r) + W(r)(k_{tb}a)\sum_{i=0}^{N}g_iU_i(r) = \frac{\sigma_m}{E_P} \tag{35a}$$

$$\frac{3(3+\nu_P)}{1+\nu_P}\sum_{i=0}^{N}\frac{(i+1)}{2}g_iU_i(r) + W(r)(k_{tb}a)\sum_{i=0}^{N}f_iU_i(r) + W(r)(k_{bb}a)\sum_{i=0}^{N}g_iU_i(r) = \frac{\sigma_b}{E_P} \tag{35b}$$

Be exploiting the discrete orthogonality of Chebyshev polynomials of the second kind, these equations can be rewritten as, after multiplying eqns (35) with $W(r)U_j(r)$ then integrating from -1 to 1,

$$A_{ij}f_j + B_{ij}g_j = \frac{\pi}{2}\frac{\sigma_0}{E_P}\delta_{0j} \quad (i,j = 0,1,2,\ldots,N) \tag{36a}$$

$$C_{ij}f_j + D_{ij}g_j = \frac{\pi}{2}\frac{\sigma_b}{E_P}\delta_{0j} \quad (i,j = 0,1,2,\ldots,N) \tag{36b}$$

where

$$A_{ij} = \tfrac{1}{4}\pi(i+1)\delta_{ij} + (k_{tt}a)\gamma_{ij} \tag{37a}$$

$$B_{ij} = (k_{tb}a)\gamma_{ij} \tag{37b}$$

$$C_{ij} = (k_{bt}a)\gamma_{ij} \tag{37c}$$

$$D_{ij} = \frac{3(3+\nu_P)\pi}{4(1+\nu_P)}(i+1)\delta_{ij} + (k_{bb}a)\gamma_{ij} \tag{37d}$$

$$\gamma_{ij} = \int_{-1}^{1} [W(r)]^2 U_i(r) U_j(r)\,\mathrm{d}r = \begin{cases} 0 & i+j \text{ is odd} \\ \dfrac{4(i+1)(j+1)}{(i+j+3)(i+j+1)(i-j+1)(j-i+1)} & i+j \text{ is even} \end{cases} \tag{37e}$$

δ_{ij} being the Kronecker delta. The proof for the explicit expression of γ_{ij} is given in Appendix C.

6.2. Reissner's plate theory

In a similar manner as described in the previous section, eqn (30b) can be expressed as

$$\frac{3}{2}\sum_{i=0}^{N}(i+1)g_iU_i(r) - \frac{15}{(1+\nu_P)2\pi}\left(\frac{a}{t_P}\right)^2 \sum_{i=0}^{N} g_i\bar{L}_i(r) + W(r)(k_{tb}a)\sum_{i=0}^{N} f_iU_i(r) + W(r)(k_{bb}a)\sum_{i=0}^{N} g_iU_i(r) = \frac{\sigma_b}{E_P} \tag{38}$$

where

$$\bar{L}_i(r) = \int_{-1}^{1} L\left(\sqrt{10}\,\frac{a}{t_P}|r-\eta|\right) W(\eta)U_i(\eta)\,\mathrm{d}\eta \tag{39}$$

Multiplying eqn (38) with $W(r)U_j(r)$ then integrating from -1 to 1, one obtains, noting that the tensile stretching equation is identical to the first of eqn (36),

$$A_{ij}f_j + B_{ij}g_j = \frac{\pi}{2}\frac{\sigma_0}{E_P}\delta_{0j} \quad (i,j = 0,1,2,\ldots,N) \tag{40a}$$

$$C_{ij}f_j + F_{ij}g_j = \frac{\pi}{2}\frac{\sigma_b}{E_P}\delta_{0j} \quad (i,j = 0,1,2,\ldots,N) \tag{40b}$$

where

$$F_{ij} = \frac{3}{4}\pi(i+1)\delta_{ij} + (k_{bb}a)\gamma_{ij} - \frac{15}{(1+\nu_P)2\pi}\left(\frac{a}{t_P}\right)^2 L_{ij} \tag{41a}$$

$$L_{ij} = \int_{-1}^{1} = \bar{L}_i(r)W(r)U_j(r)\,\mathrm{d}r \equiv \int_{-1}^{1}\int_{-1}^{1} L(\sqrt{10}|r-\eta|a/t_P)W(\eta)W(r)U_i(\eta)U_j(r)\,\mathrm{d}\eta\,\mathrm{d}r \tag{41b}$$

where A_{ij}, B_{ij}, C_{ij} and γ_{ij} are given by eqns (37). Since the kernel $L(s)$ has a logarithm singularity, the above double integration presents a major time-consuming operation for the numerical analysis. One way to attenuate this difficulty is to separate the logarithm singularity, which can be calculated in closed-form (Joseph and Erdogan, 1987),

$$\begin{aligned} L_{ij} &= \int_{-1}^{1}\int_{-1}^{1} [L(\sqrt{10}|r-\eta|a/t_P) - \ln|r-\eta| + \ln|r-\eta|]W(\eta)W(r)U_i(\eta)U_j(r)\,\mathrm{d}\eta\,\mathrm{d}r \\ &= \int_{-1}^{1}\int_{-1}^{1} [L(\sqrt{10}|r-\eta|a/t_P) - \ln|r-\eta|]W(\eta)W(r)U_i(\eta)U_j(r)\,\mathrm{d}\eta\,\mathrm{d}r + \alpha_{ij} \end{aligned} \tag{42}$$

where

$$\alpha_{ij} = \begin{cases} -\dfrac{\pi^2}{16}[1+4\ln 2] & i=j=1 \\ -\dfrac{\pi^2}{8}\left(\dfrac{1}{j-1}+\dfrac{1}{j+1}\right) & i=j=1 \\ \dfrac{\pi^2}{8(j-1)} & j=i+2 \\ \dfrac{\pi^2}{(jj+1)} & j=i=2 \\ 0 & \text{otherwise} \end{cases} \tag{43}$$

detailed derivations are given in Appendix D. The remaining integrand in eqn (42) is a smooth function everywhere within the integration interval, thus allowing the integral to be evaluated using simple quadrature rules.

The coupled linear set of eqns (36) or (40) can be readily solved for the unknown coefficients f_i and g_i, from which the membrane and bending stress intensity factors can then be determined via eqns (26), (27),(31), noting

$$\bar{h}_1(1) = \sum_{i=0}^{N} (1+i) f_i$$

$$\bar{h}(1) = \sum_{i=0}^{N} (1+i) g_i$$

Table 1 illustrates the convergence of the solutions for intermediate and long crack cases, based on Kirchhoff–Poisson plate theory. The Reissner's plate theory formulation exhibits a similar convergence. In this table the reduction in the stress intensity factor as a result of repair is calculated for different numbers of leading terms in the expansion in terms of the Chebyshev polynomials. From Table 1 it can be seen that as the crack length increases more terms are required to achieve the same degree of accuracy. For instance, for $K_{tt}a = 1.0$, a total of 32 terms is sufficient to achieve an accuracy better than 0.1%, whereas 64 terms are needed to achieve the same accuracy for $k_{tt}a = 10.0$. The main reason for this is due to the boundary layer effect in the crack face opening displacement: as the stiffness of the bridging springs increases, the crack-opening displacement becomes essentially constant over the entire crack length, except in the vicinity of the crack tips, where the crack-opening displacement sharply decreases to zero (Rose, 1987; Nemat-Nasser and Hori, 1987). However, as will be shown later, the stress intensity factors obtained for a normalised

Table 1
Convergence of solution using Kirchhoff–Poisson plate theory

N	$K_m/\sigma_m\sqrt{\pi a}$	Difference (%)	$K_b^{(K)}/\sigma_b\sqrt{\pi\alpha}$	Difference (%)
$k_{tt} = 1.0$				
2	0.720183	3.096	1.6896	4.923
4	0.732071	1.497	1.65512	2.781
8	0.739196	0.538	1.62693	1.030
16	0.742024	0.157	1.61504	0.294
32	0.742885	0.042	1.61155	0.076
64	0.743123	0.0095	1.61061	0.017
128	0.743186	0.0011	1.61037	0.002
256	0.743194	—	1.61033	—
$k_{tt}a = 10$				
2	0.301707	−16.542	0.831925	−5.417
4	0.329653	−8.8112	0.890410	1.2320
8	0.347698	−3.8196	0.906460	3.0567
16	0.356674	−1.3366	0.904024	1.6428
32	0.360270	−0.3419	0.883558	0.4529
64	0.361216	−0.0802	0.880411	0.0952
128	0.361472	−0.0094	0.879674	0.0114
256	0.361506	—	0.879574	—

Notes: 1. $k_{bt}/k_{tt} = -3.4744$, $k_{bb}/k_{tt} = 18.5263$. 2. The difference is measured relative to the value for $N = 256$ and is used as a measure of convergence of the series.

crack length of $k_{tt}a = 10.0$ is sufficiently close to the long crack limit, $k_{tt}a \to \infty$, so that no further calculations involving much higher order of expansion is necessary.

7. Results and discussion

For illustration we shall consider the case of a typical bonded repair to highlight the important ramifications of repairing unsupported structures using existing design methodology, which has been developed for symmetric repairs or well-supported one-sided repairs. The dimensions and material properties of the cracked plate, reinforcement and the adhesive layer are summarised in Table 2, which represents a typical repair that has been extensively used in practical applications (Baker and Jones, 1988). Two different loading cases will be considered separately : remote tension and remote bending. In the case of remote tension, the effect of geometrically non-linear deformation will be analysed used a hybrid method.

7.1. *Remote tension*: *geometrically linear analysis*

The plate is assumed to be subjected to a uniform tension, σ^{∞}, remotely. According to eqns (6) and (7), the prospective membrane and the maximum bending stresses acting on the crack faces are, respectively,

$$\sigma_m = \left(\frac{1}{1+S} + \frac{t_{\mathrm{P}}\bar{z}^2}{I_t}\right)\sigma^{\infty} \tag{44}$$

$$\sigma_b = \frac{t_{\mathrm{P}}^2\bar{z}}{2I_t}\sigma^{\infty} \tag{45}$$

With the material properties and dimensions given in Table 2, the coupled eqns (36) and (40), representing Kirchhoff–Poisson plate theory and Reissner's plate theory, are solved numerically. The results are plotted in Fig. 6. It is clear that the formulation based Kirchhoff–Poisson plate theory significantly over-predicts the bending stress intensity factor as compared to Reissner's plate theory, while the membrane stress intensity factors appear to be well predicted. Even when the Kirchhoff–Poisson bending stress intensity factor is converted to an equivalent Reissner bending stress intensity factor using eqn (19), Kirchhoff–Poisson plate theory prediction still

Table 2
Physical dimensions and material properties of a typical repair

Layer	Young's modulus (GPa)	Poisson's ratio	Thickness (mm)
Plate	71	0.3	3.0
Reinforcement	207	0.3	1.0
Adhesive	1.89	0.33	0.2

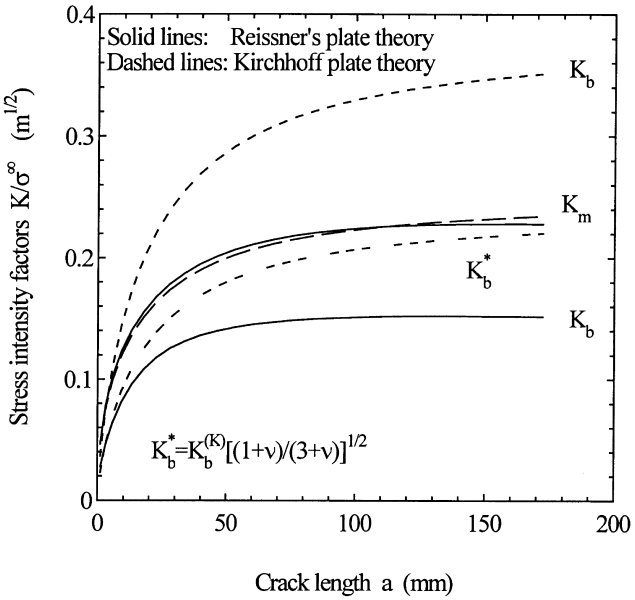

Fig. 6. Comparison of models based on Kirchhoff-Poisson plate theory and the Reissner's plate theory.

remains considerably higher than that predicted using Reissner's plate theory. The breakdown of the relationship (19) is due to the coupling between the tensile and bending springs sprung between crack faces, resulting in the inapplicability of the path-independent integral used in deriving (19). Therefore in the following analyses solutions based on Kirchhoff–Poisson plate theory will not be discussed further.

The numerical results obtained from the formulation based on Reissner's plate theory, i.e., eqn (40), are plotted in Fig. 7, together with the results of a three-dimensional finite element analysis (Callinan et al., 1997). Considering the approximate nature of the crack bridging model and the finite element method, the correlation between the predictions and the finite element results is reasonably good. Nevertheless further work is desirable to clarify the discrepancies in the short crack regime.

7.2. *Remote tension*: *geometrically non-linear analysis*

The superposition principle used in Section 2 to reduce the problem of a one-sided repair subjected to remote tension to a simple perturbation problem where the crack is internally pressurised is, strictly speaking, not valid should the structure undergo geometrically nonlinear deformation. However, an upper bound solution can be obtained by a hybrid method, in which the prospective stress distribution is solved using geometrically nonlinear elasticity theory, but the spring constants derived from a linear analysis are retained in eqns (23) and (30). A detailed proof is provided in Appendix E.

From eqns (8) and (9) the prospective and maximum bending stresses are,

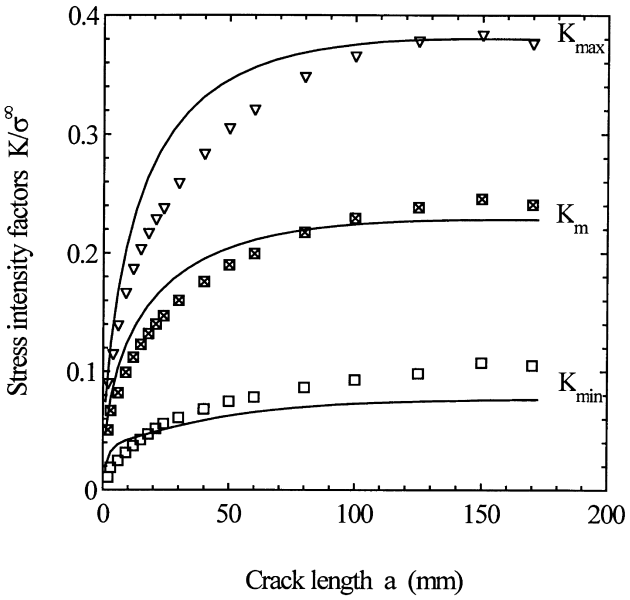

Fig. 7. Theoretical predictions and finite element results for a typical one-sided repair assuming geometrically linear-deformation.

$$\sigma_m = \frac{1}{1+S}\sigma^{\infty} \tag{46}$$

$$\sigma_b = 0 \tag{47}$$

With this stress distribution, the coupled eqns (40) are then solved numerically and the results are plotted in Fig. 8. When compared with the geometrically linear analysis, both the membrane and the bending stress intensity factors have reduced by almost a factor of two, suggesting a strong influence of the geometrically non-linear deformation on the repair efficiency of one-sided repairs. Nevertheless, the results shown in Fig. 8 also reveal that the repair efficiency of a one-sided repair is still much lower than the equivalent two-sided repairs, with the mean and maximum stress intensity factors being about twice and four times those of equivalent two-sided repairs for the geometry being considered. It is interesting to note that although the prospective maximum bending stress is zero, there is still a significant bending stress intensity factor, resulting from the coupling between the tension and bending springs.

7.3. Remote bending

Recently attempts have been made to apply the bonded repair technique to repair fatigue damage caused by acoustic vibration. Due to the pressure waves caused by engine and/or aerodynamic effects, aircraft skin structures may experience a high degree of acoustic fatigue. For example, the external surface of the lower nacelle skin of the F/A-18 aircraft has been found to experience acoustically induced cracking (Brewer, 1994). Cracking generally occurs along the longer side of

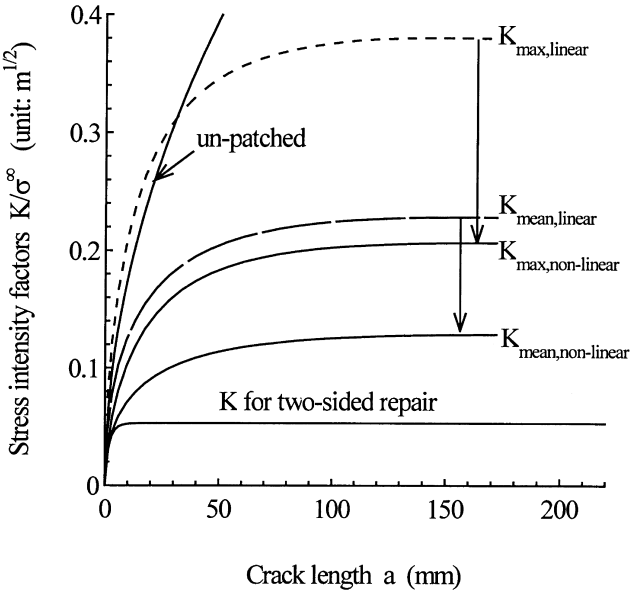

Fig. 8. Influence of geometrically non-linear deformation on the repair efficiency.

a panel where the bending stresses due to the out-of-plane vibrations are the maximum. The main feature in this case is that the cracked plate is subjected to mainly out-of-plane bending with little in-plane loading, as illustrated in Fig. 9.

Application of bonded composite repairs in this case will have two effects; firstly to reduce the panel vibration response due to the increase in stiffness and secondly to restrain the crack opening thus reducing crack driving force. In the present work we will investigate only the reduction in the crack driving force as a result of crack bridging. According to eqns (6) and (7), the membrane stress and the maximum bending stress are

$$\sigma_m = \frac{t_P^2}{6I_t}\sigma_b^\infty \tag{48}$$

$$\sigma_b = \frac{t_P^3}{12I_t}\sigma_b^\infty \tag{49}$$

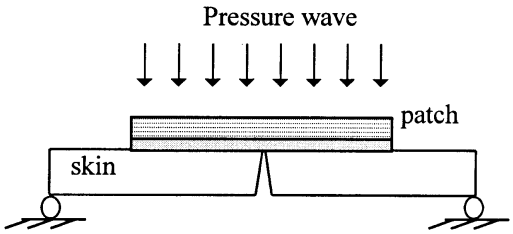

Fig. 9. Bonded repair subjected to acoustic fatigue loading.

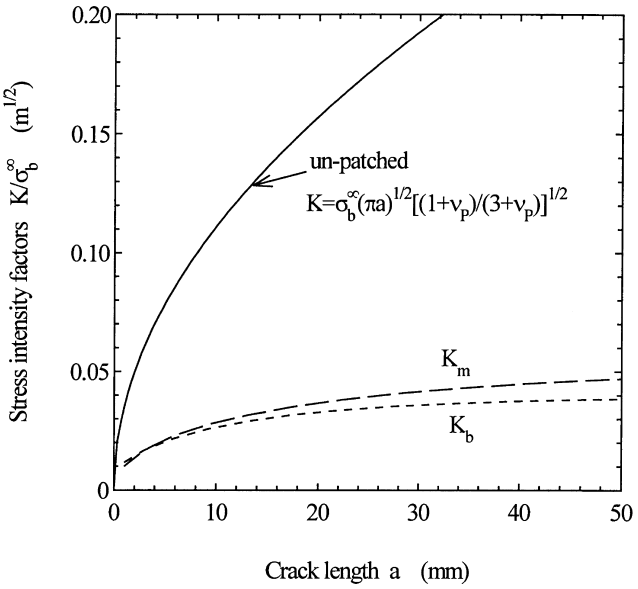

Fig. 10. Repair efficiency of one-sided repairs subjected to acoustic loading.

where σ_b^∞ represents the maximum bending stress that the panel experiences before the application of a bonded patch. With this stress distribution, the coupled eqns (40) are then solved numerically and the results are plotted in Fig. 10, indicating that the one-sided repair is also effective in the case of cracked plates being subjected to out-of-plane bending. It should be pointed out that crack closure on the compressive side, especially when the pressure depicted in Fig. 9 is reversed, is not addressed in the present work; this will be the subject of a separate article.

8. Summary and conclusions

A crack bridging model has been presented for analysing the tensile stretching and bending of a cracked plate, which is repaired on one side, subjected to tension and bending. The repaired structure is modelled as a plate containing a through thickness crack, bridged by tension and bending springs, whose stiffness constants are determined from a one-dimensional analysis of single strap joint. The results show that Kirchhoff–Poisson plate theory would considerably overestimate the bending stress intensity factor, while the formulation based Reissner's plate theory provides a reasonably good estimate of both the membrane and bending stress intensity factors, when compared with results from a three-dimensional finite element analysis. To account for the beneficial effect of geometrically nonlinear deformation on the repair efficient of one-sided repairs, a hybrid method is proposed, within the framework of a two-stage analysis. First, the prospective stresses along the crack path are determined using geometrically nonlinear elasticity theory. Secondly, the perturbation problem is solved within the framework of geometrically linear elasticity. The results show that a one-sided repair is still much less efficient in reducing the stress intensity factor than an equivalent two-sided repair.

Appendix A: Derivation of the spring compliance matrix

The governing equations for the adhesive shear and peel strains, which are assumed to be constant through the adhesive thickness, are, respectively,

$$\frac{\mathrm{d}^3\gamma^{(\mathrm{A})}}{\mathrm{d}y^3}-\beta_s^2\frac{\mathrm{d}\gamma^{(\mathrm{A})}}{\mathrm{d}y}=0 \tag{A1}$$

$$\frac{\mathrm{d}^4\varepsilon^{(\mathrm{A})}}{\mathrm{d}y^4}-4\kappa^4\varepsilon^{(\mathrm{A})}=0 \tag{A2}$$

where

$$\beta_s^2=\frac{4\mu_{\mathrm{A}}}{t_{\mathrm{A}}}\left[\frac{1}{E'_{\mathrm{P}}t_{\mathrm{P}}}+\frac{1}{E'_{\mathrm{R}}T_{\mathrm{R}}}\right]\equiv 4\beta^2 \tag{A3}$$

$$\kappa^4=\frac{E'_{\mathrm{A}}}{4t_{\mathrm{A}}}\left[\frac{1}{D_{\mathrm{P}}}+\frac{1}{D_{\mathrm{R}}}\right] \tag{A4}$$

where μ_{A} and t_{A} represent the shear modulus and the thickness of the adhesive layer, D_{P} and D_{R} refer to the bending stiffness of the plate and reinforcement, $D_{\mathrm{P,R}}=E'_{\mathrm{P,R}}\mathrm{t}^3_{\mathrm{P,R}}/12$, and $E'_{\mathrm{A}}=2\mu_{\mathrm{A}}/(1-v)$ is the Young's modulus of the adhesive under plane strain condition. The differential equation (A) has the following solution in the domain $y>0$,

$$\gamma^{(\mathrm{A})}=\gamma^{(\mathrm{A})}_{\max}\,e^{-\beta_s y} \tag{A5}$$

where $\gamma^{(A)}_{max}$ represents the maximum shear strain at $y=0$. Similarly the relevant solution for the adhesive peel stress in the case of semi-infinite overlap in the domain $y>0$ is,

$$\varepsilon^{(\mathrm{A})}=(A\cos\kappa y+B\sin\kappa y)\,e^{-\kappa y} \tag{A6}$$

The three unknowns, $\gamma^{(A)}_{\max}$ and constants A and B need to be determined from the appropriate boundary conditions.

The boundary condition for the shear strain is,

$$\begin{aligned}\left.\frac{\mathrm{d}\gamma^{(\mathrm{A})}}{\mathrm{d}y}\right|_{y=0}&=\frac{\varepsilon_{\mathrm{R}}(z=t_{\mathrm{P}}/2+t_{\mathrm{A}})-\varepsilon_{\mathrm{P}}(z=t_{\mathrm{P}}/2)}{t_{\mathrm{A}}}\\&=\frac{1}{t_{\mathrm{A}}}\left[\frac{1}{E'_{\mathrm{R}}t_{\mathrm{R}}}+\frac{1}{E'_{\mathrm{P}}t_{\mathrm{P}}}+\frac{3(t_{\mathrm{R}}+t_{\mathrm{P}})}{E'_{\mathrm{R}}t^2_{\mathrm{R}}}\right]N_0+\frac{6}{t_{\mathrm{A}}}\left[\frac{1}{E'_{\mathrm{R}}t^2_{\mathrm{P}}}-\frac{1}{E'_{\mathrm{P}}t^2_{\mathrm{R}}}\right]M_0\end{aligned} \tag{A7}$$

The relevant boundary conditions for the adhesive peel strain at $y=0$ are,

$$\left.\frac{\mathrm{d}^2\varepsilon^{(\mathrm{A})}}{\mathrm{d}y^2}\right|_{y=0}=\frac{1}{t_{\mathrm{A}}}\frac{\mathrm{d}^2(w_{\mathrm{R}}-w_{\mathrm{P}})}{dy^2}=\frac{1}{t_{\mathrm{a}}}\left(\frac{M_{\mathrm{R}}(y=0)}{D_{\mathrm{R}}}-\frac{M_{\mathrm{P}}(y=0)}{D_{\mathrm{P}}}\right)$$

$$= \frac{1}{t_A D_R}\frac{t_R + t_P}{2} N_0 + \frac{1}{t_A D_R}\left[1 + \frac{D_r}{D_P}\right] M_0 \tag{A8}$$

and

$$\left.\frac{d^3 \varepsilon^{(A)}}{dy^3}\right|_{y=0} = \frac{1}{t_A}\frac{d^3(w_R - w_P)}{dy^3} = \frac{1}{t_A}\left(\frac{V_R + \tau_{max}^{(A)} t_R/2}{D_R} - \frac{V_P + \tau_{max}^{(A)} t_P/2}{D_P}\right)$$

$$= \frac{\mu_A}{2t_A}\left(\frac{t_R}{D_R} - \frac{t_P}{D_P}\right)\gamma_{max}^{(A)} \tag{A9}$$

where the conditions that the shear force V_P and V_R are both zero at $y = 0$ have been used.

From condition (A7) one obtains

$$\gamma_{max}^{(A)} = -\frac{1}{2\beta t_A}\left[\frac{1}{E'_R t_R} + \frac{1}{E'_P t_P} + \frac{3(t_R + t_P)}{E'_R t_R^2}\right] N_0 + \frac{6}{2\beta t_A}\left[\frac{1}{E'_R t_R^2} - \frac{1}{E'_P t_P^2}\right] M_0 \tag{A10}$$

and referring to eqns (A8) and (A9) we have,

$$-2\kappa^2 B = \frac{1}{t_A D_R}\frac{t_R + t_P}{2} N_0 + \frac{1}{t_A D_R}\left(1 + \frac{D_R}{D_P}\right) M_0 \tag{A11}$$

$$2\kappa^3 (A + B) = \frac{\mu_A}{2t_A}\left(\frac{T_R}{D_R} - \frac{t_P}{D_P}\right)\gamma_{max}^{(A)} \tag{A12}$$

thus,

$$\kappa(A - B) = \frac{\mu_A t_P}{4\kappa^2 t_A}\left(\frac{t_R}{D_R} - \frac{t_P}{D_P}\right)\gamma_{max}^{(A)} + \frac{t_R + t_P}{2\kappa t_A D_R} N_0 + \frac{1}{\kappa t_A D_R}\left(1 + \frac{D_r}{D_P}\right) M_0 \tag{A13}$$

Denote the rotation of the plate at $y = 0$ as θ_0, since $\partial w_R/\partial y|_{y=0} = 0$ because of symmetry, and $\varepsilon^{(A)} = (w_R - w_P)/t_A$, we have, by definition,

$$\theta_0 = \left.\frac{\partial w_P}{\partial y}\right|_{y=0} = \left.\frac{\partial(w_P - w_R)}{\partial y}\right|_{y=0} = -t_A \left.\frac{\partial \varepsilon^{(A)}}{\partial y}\right|_{y=0} = \kappa t_A (A - B)$$

$$= \left\{\frac{t_P + t_R}{2\kappa D_R} - \frac{\mu_A}{8\kappa^2 \beta t_A}\left[\frac{t_R}{D_R} - \frac{t_P}{D_P}\right]\left[\frac{1}{E'_R t_R} + \frac{1}{E'_P t_P} + \frac{t_R(t_R + t_P)}{4D_R}\right]\right\} N_0$$

$$+ \left\{\frac{1}{\kappa D_R}\left(1 + \frac{D_R}{D_P}\right) - \frac{\mu_A}{16\kappa^2 \beta t_A}\left[\frac{t_R}{D_R} - \frac{t_P}{D_P}\right]^2\right\} M_0 \tag{A14}$$

The opening displacement at the mid-surface of the plate is,

$$
\begin{aligned}
u_0 &= -\gamma_{\max}^{(A)} t_A + \theta_0 t_P/2 \\
&= \left\{ \frac{t_P(t_R+t_P)}{4\kappa D_R} + \left[\frac{1}{E'_R t_R} + \frac{1}{E'_P t_P} + \frac{t_R(t_R+t_P)}{4D_R} \right] \left[\frac{1}{2\beta} - \frac{\mu_A t_P}{16\kappa^2 \beta t_A} \left(\frac{t_R}{D_R} - \frac{t_P}{D_P} \right) \right] \right\} N_0 \\
&\quad + \left\{ \frac{t_P}{2\kappa D_R} \left(1 + \frac{D_R}{D_P} \right) + \left[\frac{t_r}{2D_R} - \frac{t_P}{2D_P} \right] \left[\frac{1}{2\beta} - \frac{\mu_A t_P}{16\kappa^2 \beta t_A} \left(\frac{t_R}{D_R} - \frac{t_P}{D_P} \right) \right] \right\} M_0
\end{aligned} \tag{A15}
$$

It is now possible to express the crack opening displacement and crack face rotation in terms of the membrane force and the bending moment in a matrix formulation,

$$
\begin{Bmatrix} u_0 \\ \theta_0 \end{Bmatrix} = \begin{bmatrix} c_{11} & c_{12} \\ c_{21} & c_{22} \end{bmatrix} \begin{Bmatrix} N_0 \\ M_0 \end{Bmatrix} \tag{A16}
$$

where

$$
\begin{aligned}
c_{11} &= \frac{t_P(t_R+t_R)}{4\kappa D_R} + \left[\frac{1}{E'_R t_R} + \frac{1}{E'_P t_P} + \frac{t_R(t_R+t_P)}{4D_R} \right] \left[\frac{1}{2\beta} - \frac{\mu_A t_P}{16\kappa^2 \beta t_A} \left(\frac{t_R}{D_R} - \frac{t_P}{D_P} \right) \right] \\
c_{12} &= \frac{t_P}{2\kappa D_r} \left(1 + \frac{D_R}{D_P} \right) + \left(\frac{t_R}{2D_R} - \frac{t_P}{2D_P} \right) \left(\frac{1}{2\beta} - \frac{\mu_A t_P}{16\kappa^2 \beta t_A} \left(\frac{t_R}{D_R} - \frac{t_P}{D_P} \right) \right) \\
c_{21} &= \frac{t_R + t_P}{2\kappa D_R} - \frac{\mu_A}{8\kappa^2 \beta t_A} \left(\frac{t_R}{D_R} - \frac{t_P}{D_P} \right) \left(\frac{1}{E'_R t_R} + \frac{1}{E'_P t_P} + \frac{t_R(t_P+t_R)}{4D_R} \right) \\
c_{22} &= \frac{1}{\kappa D_R} \left(1 + \frac{D_R}{D_P} \right) - \frac{\mu_A}{16\kappa^2 \beta t_A} \left(\frac{t_R}{D_R} - \frac{t_P}{D_P} \right)^2
\end{aligned}
$$

It is evident that the cross terms, c_{12} and c_{21}, are non-zero, indicative of the coupling between in-plane and out-of-plane deformation. According to the Maxwell's reciprocal relation, the matrix C should be symmetric, i.e., $c_{12} = c_{21}$. However, due to the approximate nature of the plate theory, the resulting matrix is not exactly symmetric, but the deviation from symmetry is small.

Appendix B: Expansion of Fredholm kernel near singularity

Joseph and Erdogan (1987) showed that $L(z)$ is a Fredholm kernel but an error occurred in the expansion of the modified Bessel function of the second kind, hence resulting in an incorrect asymptotic expansion for small z. Correct expressions are presented below.

The small s expansion for the Bessel functions are,

$$
K_0(s) = -\ln(s/2) - \gamma_e - (s/2)^2 \ln(s/2) + O(s^2) \tag{B1}
$$

$$
K_2(s) = \frac{2}{s^2} - \frac{1}{2} + \left(\ln 2 - \ln s - \gamma_e + \frac{3}{4} \right) \frac{s^2}{8} + \left(\ln 2 - \ln s - \gamma_e + \frac{17}{12} \right) \frac{s^4}{96} + O(s^6) \tag{B2}
$$

where the Euler's constant, $\gamma_e = 0.5772157\ldots$. Substitution of these expansions into eqn (29b) leads to the following behavior for $L(s)$,

$$\lim_{z\to 0} L(s) \approx \ln(s/2) + (\gamma_e + 1/4) + (s/2)^2 \ln(s/2) + \cdots \tag{B3}$$

It is clear that the kernel $L(s)$ has only an integrable logarithm singularity.

Appendix C: Derivation of γ_{ij}

With $W(x) = \sqrt{1-x^2}$ and $U_i(x) = \sin[(i+1)\cos^{-1}(x)]/\sin(\cos^{-1}x)$, we have

$$\begin{aligned}\gamma_{ij} &= \int_{-1}^{1} W(x)W(x)U_i(x)U_j(x)\,\mathrm{d}x \\ &= \int_0^{\pi} \sin(\theta)\sin[(i+1)\theta]\sin[(j+1)\theta]\,\mathrm{d}\theta \\ &= \frac{4(i+1)(j+1)}{(i+j+3)(i+j+1)(i-j+1)(j-i+1)}\end{aligned} \tag{C1}$$

where the following identity has been used (Gradshteyn and Ryzhik, 1994)

$$\begin{aligned}&\int \sin(ax)\sin(bx)\sin(cx)\,\mathrm{d}x \\ &\quad = -\frac{1}{4}\left[\frac{\cos(a-b+c)x}{a-b+c} + \frac{\cos(b+c-a)x}{b+c-a} + \frac{\cos(a+b-c)x}{a+b-c} - \frac{\cos(a+b+c)x}{a+b+c}\right]\end{aligned} \tag{C2}$$

Appendix D: Derivation of α_{ij}

$$\begin{aligned}a_{ij} &= \int_{-1}^{1}\int_{-1}^{1} W(r)W(\eta)\ln|r-\eta|U_i(\eta)U_j(r)\,\mathrm{d}\eta\,\mathrm{d}r \\ &= \int_{-1}^{1} V_i(r)W(r)U_j(r)\,\mathrm{d}r\end{aligned} \tag{D1}$$

where

$$V_i(r) = \int_{-1}^{1} W(\eta)\ln|r-\eta|U_i(\eta)\,\mathrm{d}\eta \equiv \begin{cases} -\dfrac{\pi}{2}\left[-r^2 + \dfrac{1}{2} + \ln 2\right] & i = 0 \\ -\dfrac{\pi}{2}\left[\dfrac{T_i(r)}{i} - \dfrac{T_{i+2}}{i+2}\right] & i \geqslant 1 \end{cases} \tag{D2}$$

therefore,

$$a_{ij} = \begin{cases} -\dfrac{\pi^2}{16}[1+4\ln 2] & i=j=1 \\ -\dfrac{\pi^2}{8}\left(\dfrac{1}{j-1}+\dfrac{1}{j+1}\right) & i=j>1 \\ \dfrac{\pi^2}{8(j-1)} & j=i+2 \\ \dfrac{\pi^2}{8(j+1)} & j=i-2 \\ 0 & \text{otherwise} \end{cases} \tag{D3}$$

where the following results have been used

$$\int_{-1}^{1} T_i(x)\,W(x)\,U_j(x)\,\mathrm{d}x = \begin{cases} \pi/4 & i=j \\ -\pi/4 & i=j+2 \\ 0 & \text{otherwise} \end{cases} \tag{D4}$$

which can be proved if one uses the following identity (Gradshteyn and Ryzhik, 1994)

$$\int \cos(ax)\sin(bx)\sin(cx)\,\mathrm{d}x = \frac{1}{4}\left[\frac{\sin(a+b-c)}{a+b-c}+\frac{\sin(a+c-b)}{a+c-b}-\frac{\sin(a+b+c)}{a+b+c}+\frac{\sin(b+c-a)}{b+c-a}\right] \tag{D5}$$

Appendix E: A hybrid method for upper bound solution

Here the hybrid method refers a two-stage analysis method for solving a one-sided repair subjected to remote tension, in which the stage one is solved within the framework of geometrically nonlinear elasticity while the stage two (perturbation problem) is solved assuming the repaired region deforms geometrically linearly. It will be shown below that the proposed hybrid method will (1) correctly predict the membrane force carried by the reinforcement and (2) provide an upper-bound to the bending moment in the reinforcement, hence proving that the hybrid method will always provide a conservative prediction of the stress intensity factors.

Referring to Fig. 4(c), in the case of geometrically nonlinear deformation, the membrane force in the patch just above the crack is,

$$N_{\text{patch}} \equiv N^{\infty} \tag{E1}$$

which results directly from an equilibrium consideration. In other words, the net force that the reinforcement is carrying is equal to N^{∞}.

In the limiting case of finite overlap, geometrically nonlinear deformation of the uncracked structure depicted in Fig. 4(b) will lead the neutral plane of the reinforced section to align with the load path, as the bending moment at $x=0$ must be zero to maintain equilibrium. This implies that the vertical movement of the reinforced region is equal to $-\bar{z}$ (bar). For the cracked geometry

shown in Fig. 4(c), the loss of local bending stiffness at $x = 0$ would obviously cause the reinforced region to move further downward. Let us denote this extra displacement as Δ (<0). The bending moment in the patch just above the crack is now given by

$$M_{\text{patch}} = \left(\frac{t_P + t_R}{2} - \bar{z} + \Delta\right) N^{\infty} = \left(\frac{t_P + t_R}{2}\frac{1}{1+S} + \Delta\right) N^{\infty} \tag{E2}$$

where eqn (3) has been used.

Now if we follow the hybrid method, referring to Fig. 5(a) where N_0 and M_0 being given by eqns (6) and (7), the membrane force in the patch determined via the hybrid method, N^*_{patch}, is,

$$N^*_{\text{patch}} = N_1 + N_0 \equiv N^{\infty} \tag{E3}$$

where N_1 represents the net force in the reinforcement before the appearance of the crack, equal to

$$\int_{t_P/2}^{t_P/2 + t_R} \sigma_0(z)\,\mathrm{d}z.$$

Therefore, the membrane force as determined by the hybrid method is exactly equal to the actual force carried by the reinforcement.

The bending moment determined by the hybrid method, M^*_{patch}, is

$$M^*_{\text{patch}} = \frac{t_P + t_R}{2} N_0 = \frac{t_P + t_R}{2}\frac{N^{\infty}}{1+S} \tag{E4}$$

Comparison with eqn (E2) it is easily seen that, because $\Delta < 0$, the hybrid method always predicts a higher than actual bending moment, i.e., $M^*_{\text{patch}} \geqslant M_{\text{patch}}$. Therefore, the proposed hybrid method implies that the springs would carry a higher than actual bending moment, hence it ought to provide an upper-bound to the stress intensity factors of a one-sided repaired crack undergoing geometrically nonlinear deformation.

References

Arendt, C., Sun, C.T., 1994. Bending effects of unsymmetric adhesively bonded composite repairs on cracked aluminium panels. Proceedings of FAA/NASA International Symposium on Advanced Structural Integrity Methods for Airframe Durability and Damage Tolerance. NASA Conference Publication 3274, Part 1, pp. 33–48.

Baker, A.A., 1993. Repair efficiency in fatigue-cracked aluminium components reinforced with Boron/Epoxy patches. Fatigue Fract. Engng. Mater. Struct. 16(7), 753–765.

Baker, A.A., 1995. Bonded composite repair of metallic aircraft components—overview of Australian activities. In: Composite Repair of Military Aircraft Structures. AGARD-CP-550.

Baker, A.A., 1997. On the certification of bonded composite repairs to primary aircraft structures. Proc. 11th Int. Conf. Composite Materials. Gold Coast, Australia, pp. 1–24.

Baker, A.A., Jones, R. (ed), 1988. Bonded Repair of Aircraft Structures. Martinus Nijhoff Publishers.

Brewer, T.K., 1994. F/A A/B/C/D aircraft lower nacelle skin acoustic and strain measurements and sonic fatigue analysis. McDonnel Douglas Aerospace Report, No. MDC 94b0044.

Callinan, R., Rose, L.R.F., Wang, C.H., 1997. Three-dimensional stress analysis of crack patching. Advances in Fracture 4, 2151–2158. Pergamon Press.

Erdogan, F., Arin, K., 1972. A sandwich plate with a part-through and debonding crack. Engineering Fracture Mechanics 4, 449–458.

Frenkel, A., 1983. A Chebyshev expansion of singular integrodifferential equations with a $\partial^2 \ln|s-t|/\partial s\,\partial t$ kernel. J. Computational Physics 51, 335–342.

Gere, J.M., Timoshenko, S.P., 1987. Mechanics of Materials. 3rd ed. Chapman and Hall, London.

Golberg, M.A., 1983. The convergence of several algorithms for solving integral equations with finite-part integrals. J. Integral Equations 5, 329–340.

Golberg, M.A.,1985. The convergence of several algorithms for solving integral equations with finite-part integrals, II. J. Integral Equations 9, 267–275.

Gradshteyn, I.S., Ryzhik, I.M., 1994. Table of Integrals, Series, and Products, 5th ed. Academic Press.

Hadamard, J., 1952. Lecture on Cauchy's Problem in Linear Partial Differential Equations. Dover, New York.

Hartranft, R.J., Sih, G.C., 1968. Effect of plate thickness on the bending stress distribution around through cracks. J. Mathematics and Physics 47, 276–291.

Hui, C.Y., Zehnder, A.T., 1993. A theory for the fracture of thin plates subjected to bending and twisting moments. Int. J. Fracture 61, 211–299.

Joseph, P.F., Erdogan, F., 1987. Plates and shells containing a surface crack under general loading conditions. NASA Contractor Report 178323, NASA Langely Research Center, U.S.A.

Joseph, P.F., Erdogan, F., 1989. Surface crack problems in plates. Int. J. Fracture 41, 105–131.

Keer, L.M., Lin, C.T., Mura, T., 1976. Fracture analysis of adhesively bonded sheets. Journal of Applied Mechanics 98(4), 652–656.

Knowles, J.K., Wang, N.M., 1960. On the bending of an elastic plate containing a crack. J. Math. and Phys. 39, 233.

Nemat-Nasser, S., Hori, M., 1987. Toughening by partial or full bridging of cracks in ceramics and fibre reinforced composites. Mechanics of Materials 6, 245–269.

Ratwani, M.M., 1979. Cracked, adhesively bonded laminated structures. AIAA Journal 17(9), 988–994.

Reissner, E., 1947. On bending of elastic plates. Quarterly J. Applied Mathematics 5, 55–68.

Rice, J.R., Levy, N. 1972. The part-through surface crack in an elastic plate. J. Appl. Mech. 39, 185–194.

Rose, L.R.F., 1981. An application of the inclusion analogy for bonded reinforcements. Int. J. Solids and Structures 17, 827–838.

Rose, L.R.F., 1982. A cracked plate repaired by bonded reinforcements. Int. J. Fracture 18(2), 135–144.

Rose, L.R.F., 1987. Crack reinforcement by distributed springs. J. Mech. Phys. Solids 35(4), 383–405.

Rose, L.R.F., 1988. Theoretical analysis of crack patching. In : Baker, A.A., Jones R. (Eds.), Bonded Repair of Aircraft Structures. Martinus Nijhoff Publishers, pp. 77–105.

Rose, L.R.F., Callinan, R.J., Baker, A.A., Sanderson, S., Wilson, E.S., 1995. Design validation for a bonded composite repair to the F-111 lower wing skin. Proceedings of 2nd Pacific International Conference on Aerospace Science and Technology 1, 333–336.

Sih, G.C., 1971. A review of the three-dimensional stress problem for a cracked plate. Int. J. Fracture 7(1), 39–61.

Timoshenko, S.P., Woinowsky-Krieger, S., 1959. Theory of plates and shells. McGraw-Hill.

Wang, C.H., Rose, L.R.F., 1997. On the design of bonded patches for one-sided repair. Proc. 11th International Conference on Composite Materials, Gold Coast, Australia, 5, 347–356.

Wang, C.H., Rose, L.R.F., 1998. Bonded repair of cracks under mixed mode loading. Int. J. Solids and Structures 35(21), 2749–2773.

Wang, C.H., Callinan, R.J., Rose, L.R.F., 1998. Analysis of out-of-plane bending of one-sided repair. Int. J. Solids and Structures 35(14), 1653–1675.

Wang, N.M., 1968. Effects of plate thickness on the bending of an elastic plate containing a crack. J. Math. Physics 47, 371–390.

Williams, M.L., 1961. The bending stress distribution at the base of stationary crack. J. Applied Mechanics 28, 78–82.